Graded-index optical fiber transverse-spatial-mode entanglement

Çağın Ekici * and Mehmet Salih Dinleyici
Department of Electrical and Electronics Engineering, Izmir Institute of Technology, 35430 Izmir, Turkey

(Received 16 April 2020; accepted 2 June 2020; published 6 July 2020)

We present a study of spontaneously arisen spatially entangled photon pairs via intermodal four-wave mixing in a graded-index multimode optical fiber. Unique dispersive features of the fiber allow spectral indistinguishability of two different phase-matched processes, producing entangled pairs of spatial qubits. The bases are realized as superpositions of orthogonal transverse fiber modes having opposite parities. In particular, we take into consideration the spectral properties of the processes by examining their joint spectral amplitudes. It is shown that illuminating graded-index optical fiber with different pump wavelengths has an impact upon efficiency parameters accordingly the degree of spatial entanglement and gives rise to photon pairs with various spectral purities. Photons with higher spectral purity enable desired single-photon based interactions to take place, whereas photons with lower spectral purity exhibit hybrid entanglement in frequency and transverse mode. We also discuss Wigner function formalism and parity-displacement-based realization to characterize spatial properties of the states, as well as to verify quantum entanglement through a violation of Clauser-Horne-Shimony-Holt inequality.

DOI: 10.1103/PhysRevA.102.013702

I. INTRODUCTION

Quantum information technologies are the subject of sustained interest and development efforts, and they continue to emerge with promising and striking findings. Among these technologies, photon-based implementations find a great number of applications. Depending on the application, photons with specific quantum states, from uncorrelated to entangled in a degree of freedom, should serve the purpose. Thus far, polarization and spectral degrees of freedom of generated photons are studied extensively. Polarization-entangled photons [1,2], quantum-correlated photons with a spectral degree of freedom created by engineering particular properties of the medium and pump field [3–5], are prepared. However, the amount of quantum information per photon can be increased by enhancing individually manageable and measurable number of degrees of freedom. Therefore, together with spectral (temporal) and polarization degrees of freedom, quantum information can also be encoded transverse-spatial modes of the photon.

To generate photons with specific quantum states, the well-established process of spontaneous parametric down-conversion (SPDC) in crystals having nonzero $\chi^{(2)}$ nonlinearity is used traditionally. In these bulk crystals, the transverse profile of photons can be described by continuous variables, and hence they need a special treatment known as Schmidt decomposition, in which the joint state is written as a discrete summation [6,7], whereas inside a guided-wave structure they are naturally defined in terms of a discrete set of spatial modes. Recently, a 1-mm-long multimode nonlinear periodically polled $\chi^{(2)}$ waveguide is studied to generate and characterize spatial qubits [8]. On the other hand, the process of spontaneous four-wave mixing (sFWM) based on $\chi^{(3)}$ nonlinearity of the optical fiber is a powerful alternative to SPDC, since efficient coupling into other communication components is desirable for practical photon sources, particularly for quantum communications applications where they may need to be transmitted over long distances. Step-index optical fibers [9] and bow-tie fibers [10] are utilized as photon-generation platforms in different spatial modes by exploiting intermodal phase matching. Apart from these optical fibers, graded-index multimode optical fibers (GIMFs) have unique properties that allow all the modes having the same principal mode number to propagate with nearly identical propagation constants as the result of the Wentzel, Kramers, and Brillouin (WKB) approximation [11]. These mode groups are used as individual transmission channels to reach very high bandwidths in classical communication [12], while in quantum optics the generation of frequency-degenerate photons in the same mode group may provide an opportunity for spatially entangled photon pair generation.

In this paper, we analyze theoretically generation of photon pairs in GIMF as a source of spectral and spatial correlated qubits in every aspects. In Sec. II, we present a brief overview of GIMFs and mode groups with degenerate propagation constants. Photon pairs generation via intermodal sFWM are examined in details in Sec III. Various degrees of spatially entangled states having different spectral purities are shown in Sec. IV to respond to every need in photon-based quantum information technologies. Section V focuses on characterization of spatial qubits to identify basis modes by means of Wigner function formalism and its realization based on simple interferometer with a geometric phase rotator. Violation of the Clauser-Horne-Shimony-Holt (CHSH) inequality [13] is demonstrated in Sec. VI as a verification of entanglement with the extension of the proposed experimental method in the previous section. Finally, we draw conclusions and discuss future prospects in Sec. VII.

*caginekici@iyte.edu.tr

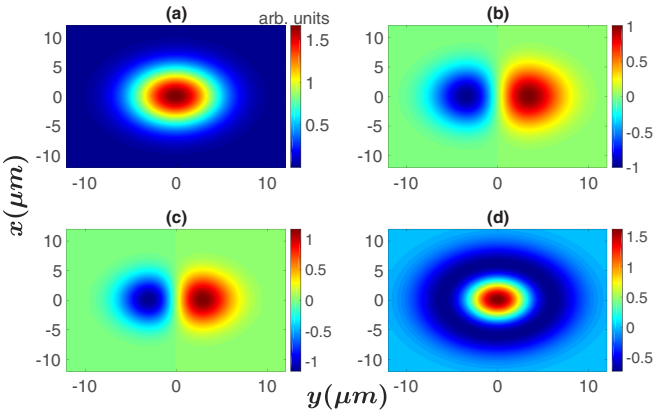

FIG. 1. Real part of the transverse field component of the optical fiber modes (a) LP_{01} and (b) LP_{11} at 600 nm, (c) LP_{11} at 460 nm, and (d) LP_{02} at 633 nm.

II. GRADED-INDEX MULTIMODE FIBERS

Cylindrically symmetric refractive index profile of the optical fibers is given by the well-known piecewise equation

$$n^2(r) = \begin{cases} n_1^2\left[1 - 2\Delta\left(\frac{r}{R}\right)^{\alpha}\right], & 0 \leqslant r \leqslant R \\ n_1^2[1-2\Delta] = n_2^2, & r > R \end{cases},$$

where R is the core radius, n_1 is the maximum refractive index in the center of the core, n_2 is the cladding refractive index, and Δ is the guidance parameter that indicates the refractive index difference between the core and cladding as $\Delta = (n_1^2 - n_2^2)/2n_2^2$.

For a GIMF having parabolic index profile $\alpha \approx 2$, the transverse electric-field distribution of a propagation invariant scalar mode (eigen-function) written as [14]

$$F_{\mathrm{m,p}}(r,\phi) = \sqrt{\frac{(p-1)!}{\pi(p-1+|m|)!}}\frac{r^{|\mathrm{m}|}}{r_0^{|\mathrm{m}|+1}}L_{\mathrm{p-1}}^{|\mathrm{m}|}\left(\frac{r^2}{r_0^2}\right) \times \exp\left(-\frac{r^2}{2r_0^2}\right)e^{im\phi} \quad (1)$$

with

$$r_0 = \sqrt{R}/\left(2k_0^2 n_1^2 \Delta\right)^{1/4},$$

where $L_{\mathrm{p}}^{|\mathrm{m}|}$ is the generalized Laguerre polynomials, and $k_0 = 2\pi/\lambda$. Here each propagation-invariant mode is characterized by two indices (m, p) referred to the angular and radial numbers, where m is an integer and $p \in \mathbb{Z}^+$, respectively. Note that for the linearly polarized (LP) modes under weak guiding approximations, which suggests that transverse modes are essentially polarized in one direction, for small Δ, the longitudinal component of the electric field is small compared to the transverse component. Accordingly, Eq. (1) represents the dominant component of the electric field. Exemplary real part of the transverse electric fields are plotted in Fig. 1. In our notation, the spatial mode profile of an LP mode is characterized by $LP_{|\mathrm{m}|\mathrm{p}}$.

GIMFs offer many advantages in terms of nonlinear interactions due to almost degenerate propagation constant values among modes with equal mode group number $g = 2p + |m| - 1$, approximated by the WKB method as [14]

$$\beta_g = n_1 k_0\{1 - 2\Delta[g/\sqrt{N_\alpha}]^{2\alpha/(\alpha+2)}\}^{1/2}, \quad (2)$$

where the number of guided modes N_α is defined as

$$N_\alpha = \frac{\alpha}{\alpha+2}k_0^2 n_1^2 R^2 \Delta. \quad (3)$$

III. FOUR-WAVE MIXING AND PHOTON PAIR GENERATION

sFWM is a $\chi^{(3)}$ parametric nonlinear process that involves the interaction of four optical waves. For the photon pair generation processes, two pump photons (p_1 and p_2) are annihilated to generate a signal (s) and idler (i) photon pair. In order for this process to take place, energy and momentum must be conserved. In optical terms, omitting $\hbar$, the conservation rules equate total frequencies and match total phases of annihilated photons and those of created photons. The phase-matching condition depends simply on the propagation constants of the participating fields, which are determined by the frequency (energy), geometry, and the refractive index profile of the optical fiber under consideration. There are two prevalent techniques for achieving phase matching in single-mode fibers: exploiting birefringence [15,16] and setting the pump wavelength close to the zero dispersion wavelength region [17,18]. However, in multimode fibers, phase-matching conditions become diversified due to multiple transverse modes with different dispersive properties and propagation constants [19]. In multimode optical fibers, the phase-matching condition, known as intermodal phase matching, is written as

$$\Delta\beta = \beta_s^{\gamma}(\omega_s^0) + \beta_i^{\kappa}(\omega_i^0) - \beta_{p_1}^{\mu}(\omega_{p_1}^0) - \beta_{p_2}^{\nu}(\omega_{p_2}^0). \quad (4)$$

Here $\beta_j^{\Gamma}(\omega_j^0)$ represents the propagation constant of the jth field with the center frequency ω_j^0 and spatial mode Γ, $j \in \{p_1, p_2, s, i\}$. In order to find phase-matching points, routine Taylor expansion of Eq. (4) up to second order is utilized about the central frequency $\omega_0 = (\omega_{p_1}^0 + \omega_{p_2}^0)/2$, regarding energy conservation, $\omega_s^0 + \omega_i^0 - \omega_{p_1}^0 - \omega_{p_2}^0 = 0$.

From the standard perturbative approach of sFWM inside multimode optical fiber, the total biphoton quantum state subjected to heralding measurement is the sum of all possible N phase-matched processes ($\Delta\beta \approx 0$), as follows:

$$|\Psi_t\rangle = \sum_{j=1}^{N}\eta_j \int d\omega_s d\omega_i f_j(\omega_s,\omega_i;\tau_j)\hat{a}_s^{\dagger}(\omega_s;\mu_j) \times \hat{a}_i^{\dagger}(\omega_i;\nu_j)|0\rangle_s|0\rangle_i, \quad (5)$$

and for each process j, η_j represents the probability amplitude that depends on the relevant $\chi^{(3)}$ nonlinear susceptibility, the fiber length L, pump powers, and spatial overlap integral. The normalizable joint spectral amplitude (JSA), $f_j(\omega_s,\omega_i;\tau_j)$ of the process j, has a simple physical meaning: The modulus squared of the normalized JSA, $|f_j^n(\omega_s,\omega_i;\tau_j)|^2$, gives a joint probability density to detect a signal photon with a frequency ω_s and a corresponding idler photon with a frequency ω_i with a possible time delay τ_j between nondegenerate pump fields (for processes triggered by degenerate pump fields $\tau_j =$

0). Here, $\hat{a}_s^\dagger(\omega;\mu_j)$ $[\hat{a}_i^\dagger(\omega;\nu_j)]$ is the photon creation operator, which generates signal (idler) photons with frequency ω and spatial mode $\mu_j(\nu_j)$, and $|0\rangle_s|0\rangle_i$ is the two-mode vacuum state. It should be emphasized that generation of two-dimensional modal entangled quantum states is provided by substantial overlap of two different phase-matched processes in the spectral domain, i.e., $f_l(\omega_s,\omega_i;\tau) \approx f_j(\omega_s,\omega_i;\tau)$ for $l \neq j$ [20].

IV. SPECTRAL PROPERTIES OF PHASE MATCHED PROCESSES

As the basis states for the spatial qubits, single photons are prepared in LP_{01} and LP_{11} modes whose electric field distributions are shown in Fig. 1. Selection of this basis gives an opportunity to use stable mode sorting based on the parity of the transverse-spatial states at the single-photon level [21]. As we show in Sec. VI, CHSH spatial violation is based on the spatial Wigner function and correlated photons subjected to two particular inverting interferometers [22].

Simultaneous realization of two phase-matched processes sharing a common spectral band are considered to produce the state

$$|\Psi\rangle = \int d\omega_s d\omega_i [\eta_1 f_1(\omega_s,\omega_i;\tau)|\omega_s;\mathrm{LP}_{11}\rangle|\omega_i;\mathrm{LP}_{01}\rangle + \eta_2 f_2(\omega_s,\omega_i;\tau)|\omega_s;\mathrm{LP}_{01}\rangle|\omega_i;\mathrm{LP}_{11}\rangle]. \quad (6)$$

The efficiency parameter η is directly proportional to spatial overlap integral of the involved modes having same polarization, $\mathcal{I} = \mathcal{I}_r\mathcal{I}_\phi$, in terms of radial $\mathcal{I}_r$ and azimuthal parts $\mathcal{I}_\phi$ as follows:

$$\mathcal{I}_r = \int_0^\infty r dr F_{p_1}^*(r)F_{p_2}^*(r)F_s(r)F_i(r), \quad (7)$$

$$\mathcal{I}_\phi = \int_0^{2\pi} d\phi \exp[-i(m_{p_1}+m_{p_2}-m_s-m_i)\phi], \quad (8)$$

where an asterisk (*) represents complex conjugation. The overlap integral is zero, once the integrand is not azimuthally symmetric; i.e., angular momentum is not conserved [10]. In order to have a nonzero overlap integral, the integrand of Eq. (8) should be equal to one, meaning that the angular mode numbers of the pumps, signal, and idler photons satisfy the selection rule for the LP modes and conserve the angular momentum [23]. Therefore, the most natural candidates for the pumps to produce state $|\Psi\rangle$ are the lowest order LP_{11} and LP_{02} modes; see Fig. 1. This nondegeneracy of the pump photons increases number of processes provided that angular momentum is conserved. It is worth stressing, to avoid confusion, that all the processes which include annihilation of two LP_{11} pump photons, annihilation of one LP_{11} photon and one LP_{02} photon, and annihilation of two LP_{02} pump photons can contribute to output state $|\Psi_t\rangle$.

Without loss of generality, in accordance with Eq. (8), the following are true: (i) *Annihilation of two* LP_{02} *pump photons* centered at ω_{02} frequency may trigger processes $\eta_{q,p}|\omega_{s_q};\mathrm{LP}_{|m_s|q}\rangle|\omega_{i_p};\mathrm{LP}_{|m_i|p}\rangle$ conserving angular momentum, satisfying the constraint $m_s+m_i=0$, at the different phase matched frequencies ω_{s_q} and ω_{i_p} with a probability amplitude $\eta_{q,p}$. (ii) *Annihilation of two* LP_{11} *pump photons* centered at ω_{11} frequency can contribute to total quantum state by generating processes of the form $\eta_{m_s^\backslash,q^\backslash,m_i^\backslash,p^\backslash}|\omega_{s_{m_s^\backslash q^\backslash}};\mathrm{LP}_{|m_s^\backslash|q^\backslash}\rangle|\omega_{i_{m_i^\backslash p^\backslash}};\mathrm{LP}_{|m_i^\backslash|p^\backslash}\rangle$ conserving angular momentum, satisfying the constraint $m_s^\backslash + m_i^\backslash = 2$ or 0, at the different phase-matched frequencies $\omega_{s_{m_s^\backslash q^\backslash}}$ and $\omega_{i_{m_i^\backslash p^\backslash}}$ with an efficiency parameter $\eta_{m_s^\backslash,q^\backslash,m_i^\backslash,p^\backslash}$. (iii) One LP_{02} photon centered at ω_{02} frequency and one LP_{11} photon centered at ω_{11} frequency can trigger processes $\eta_{m_s',q',m_i',p'}|\omega_{s_{m_s'q'}};LP_{|m_s'|q'}\rangle|\omega_{i_{m_i'p'}};\mathrm{LP}_{|m_i'|p'}\rangle$ conserving angular momentum, satisfying the constraint $m_s'+m_i'=1$, at the different phase matched frequencies $\omega_{s_{m_s'q'}}$ and $\omega_{i_{m_i'p'}}$ with a probability amplitude $\eta_{m_s',q',m_i',p'}$. Therefore, some processes can be distinguished spectrally due to the fact that they are triggered at different phase-matched points. On the other hand, spectrally indistinguishable processes having different modal characteristics can possess nonclassical correlation in the spatial domain. Furthermore, similar values of spatial mode indices (m_s, q, m_i, p,...) have relatively high efficiency parameters η due to substantial overlap in the transverse plane. Before moving on, two points deserve to be highlighted without compromising the generality of the results: (i) Expressing the azimuthal dependence of the LP modes in a $\{\sin(m\phi), \cos(m\phi)\}$ basis dictates parity-conservation rules [10], and (ii) all the aforementioned processes may not satisfy phase-matching conditions owing to the dispersive properties of the media, notwithstanding angular momentum and parity conservations.

For simplicity, we consider only annihilation of spatially nondegenerate pump photons generating the separated state $|\Psi\rangle$ via spectral filters to present possible two-dimensional spatial entanglement.

We now turn to the study of the spectral bandwidth of photons due to finite bandwidth of the pump pulses and fiber of finite length. All these effects are embedded in the unnormalized JSA, which can be expressed as the product of pump envelope function $\alpha(v_s,v_i)$ and phase-matching function $\Phi(v_s,v_i)$ in terms of frequency detunings $v_{s,i}=\omega_{s,i}-\omega_{s,i}^0$ at perfect phase-matched frequencies $\omega_{s,i}^0$ [24]:

$$f(v_s,v_i;\tau) = \alpha(v_s,v_i)\Phi(v_s,v_i;\tau), \quad (9)$$

with

$$\alpha(v_s,v_i) = \exp\left[-\frac{(v_s+v_i)^2}{\sigma_1^2+\sigma_2^2}\right], \quad (10)$$

and

$$\Phi(v_s,v_i;\tau) = \exp\left[-\left(\frac{T_s v_s + T_i v_i}{\sigma\tau_p}\right)^2\right] \times\left[\mathrm{erf}\left(\frac{\sigma(\tau+\tau_p)}{2}+i\frac{T_s v_s+T_i v_i}{\sigma\tau_p}\right) - \mathrm{erf}\left(\frac{\sigma\tau}{2}+i\frac{T_s v_s+T_i v_i}{\sigma\tau_p}\right)\right]; \quad (11)$$

group delays are given by

$$\tau_{s,i} = L\left(\frac{\beta'_{p_1}(\omega_{p_1}^0)+\beta'_{p_2}(\omega_{p_2}^0)}{2} - \beta'_{s,i}(\omega_{s,i}^0)\right) \quad (12)$$

$$\tau_p = L\left(\beta'_{p_1}(\omega_{p_1}^0) - \beta'_{p_2}(\omega_{p_2}^0)\right) \quad (13)$$

TABLE I. Phase-matching points, normalized efficiency parameters, and spectral purities for Cornings InfiniCor eSX+.

Cfg	Prcs	p1, λ_{p_1} (nm)	p2, λ_{p_1} (nm)	λ_i (nm)	λ_s (nm)	$\lvert\eta\rvert^2$	$\mathcal{P}$ (%)
1	a	LP_{11}, 460	LP_{02}, 633	478.005	601.806	0.45	94.93
	b	LP_{11}, 460	LP_{02}, 633	478.008	601.801	0.55	94.97
2	a	LP_{11}, 488	LP_{02}, 640	518.583	594.049	0.47	80.05
	b	LP_{11}, 488	LP_{02}, 640	518.582	594.05	0.53	80.16
3	a	LP_{11}, 510	LP_{02}, 650	571.5	571.5	0.5	35.2
	b	LP_{11}, 510	LP_{02}, 650	571.5	571.5	0.5	35.2

with inverse group velocities $\beta'_\mu = d\beta_\mu(\omega)/d\omega|_{\omega^0_\mu}$, $\mu \in \{p_1, p_2, s, i\}$, $T_{s,i} = \tau_{s,i} + \frac{1}{2}\tau_p(\sigma_1^2 - \sigma_2^2)/(\sigma_1^2 + \sigma_2^2)$, and effective bandwidth $\sigma = \sigma_1\sigma_2/\sqrt{\sigma_1^2 + \sigma_2^2}$. Pumps are considered here as Gaussian spectral envelopes centered at phase-matched frequencies $\omega^0_{p_1}(\omega^0_{p_2})$ with bandwidth (half width at $1/e$ max amplitude) σ_1 (σ_2). The probability $p(\tau)$ that a photon pair is generated, $p(\tau) = |\eta|^2 \int dv_s dv_i |f(v_s, v_i; \tau)|^2$, is given by [25]

$$p(\tau) = p_{\max}\left[\frac{\operatorname{derf}\left(\frac{\sigma\tau+\sigma\tau_p}{\sqrt{2}}\right) - \operatorname{erf}\left(\frac{\sigma\tau}{\sqrt{2}}\right)}{\operatorname{erf}\left(\frac{\sigma\tau_p}{2\sqrt{2}}\right) - \operatorname{erf}\left(-\frac{\sigma\tau_p}{2\sqrt{2}}\right)}\right], \tag{14}$$

where $p_{\max}$ corresponds to the maximum generation probability, which occurs when two pumps maximally overlap in the middle of the optical fiber, $\tau = -\tau_p/2$. In this scheme based on nondegenerate pump pulses, expressed as $|\sigma\tau_p| \gg 1$, there is no interaction at the beginning of the optical fiber as the two pump pulses are temporally well separated (the slow pump is sent ahead of the fast by a time $|\tau_p/2|$), and interaction strength gradually increases when the fast pump pulse catches up to the slower pump pulse. The interaction then starts decreasing and completely vanishes once the pump pulses separate. This regime emerges as a result of short pulse durations or group velocity mismatch (temporal walk-off), which is crucial for practical implementation. Under these circumstances, the phase-matching function is reduced to

$$\Phi_{nd}(v_s, v_i) = \exp\left[-\left(\frac{T_s v_s + T_i v_i}{\sigma\tau_p}\right)^2\right]. \tag{15}$$

For a given JSA, the spectral correlation between created signal and idler photons can be calculated after decomposing into Schmidt modes as [26]

$$f(\omega_s, \omega_i) = \sum_n \varrho_n g_n(\omega_s) h_n(\omega_i), \tag{16}$$

where $g_n(\omega_s)$ and $h_n(\omega_i)$ are sets of orthogonal spectral modes with real amplitude coefficients ϱ_n. By virtue of the decomposition, one can define broadband photon wave-packet creation operators [27]

$$\hat{s}_n^\dagger = \int d\omega_s\, g_n(\omega_s)\hat{a}^\dagger(\omega_s), \tag{17}$$

$$\hat{i}_n^\dagger = \int d\omega_i\, h_n(\omega_i)\hat{a}^\dagger(\omega_i). \tag{18}$$

In terms of photon wave-packet creation operators, the two-photon state produced by sFWM postselected jth process is obtained as

$$|\Psi_j\rangle = \sum_n \varrho_{j_n}\, \hat{s}^\dagger_{j_n}\, \hat{i}^\dagger_{j_n}\, |0\rangle_s|0\rangle_i. \tag{19}$$

Because of the normalization, the probability of two-photon emission in the nth spectral mode pair is $\varrho^2_{j_n}$. Therefore, the decomposition quantifies precisely the degree of factorability (purity) by means of Schmidt number $\mathcal{K}$ or spectral purity $\mathcal{P}$ as [28]

$$\mathcal{K} = \frac{1}{\mathcal{P}} = \frac{1}{\sum_n \varrho^4_{j_n}}. \tag{20}$$

Following the investigation of nondegenerate JSA with Schmidt modes, we use realistic commerical grade GIMF such as Corning InfiniCor eSX+ as a photon pair generation platform in simulations. The typical core radius $R = 25\,\mu$m, maximum doping in weight percentage at the center of the core is 10.8 [29], and generalized Sellmeier coefficients can be found depending on the doping percentage [30]. Gaussian envelope pump fields with 1-THz bandwidths (equal to 1 nm at 532 nm) at given wavelengths are chosen to conduct experiments easily within the boundaries of current marketing of photonics and laser technology products. In Table I, we show the normalized sFWM efficiencies of different phase-matching configurations with their purities. Three configurations for the six different phase-matching processes corresponding to three spectrally distinguishable spatially identical quantum states are given, to show possibility of realizing states with different efficiency parameters which determine the degree of entanglement.

In order to distinguish synchronic realization of the frequency-degenerate two phase-matched processes sharing a common spectral band, we label first one as process a and the subsequent part is labeled as process b:

$$|\Psi\rangle = \int d\omega_s d\omega_i \Big[\underbrace{\eta_1 f_a(\omega_s, \omega_i)|\omega_s; \mathrm{LP}_{11}\rangle|\omega_i; \mathrm{LP}_{01}\rangle}_{\textit{process a}} + \underbrace{\eta_2 f_b(\omega_s, \omega_i)|\omega_s; \mathrm{LP}_{01}\rangle|\omega_i; \mathrm{LP}_{11}\rangle}_{\textit{process b}}\Big]. \tag{21}$$

Generated quantum states from first two configurations are nonmaximally entangled states which find themselves a number of applications [31]. However, the lattermost state is known as maximally entangled Bell state, i.e., $|\eta_1| = |\eta_2| = 1/\sqrt{2}$. This state possesses relatively high nonclassical correlation also in spectral domain as a result of low spectral purity. By an important extension, in this scheme, photon pairs are born with hybrid entanglement in spectral and in spatial mode.

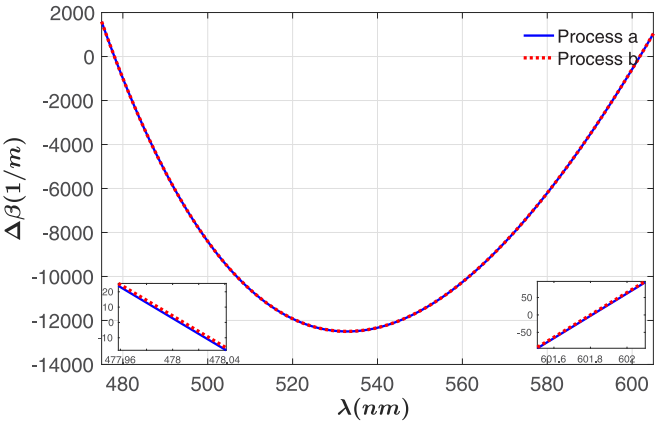

FIG. 2. Phase-matching curves for processes a and b of first configuration with phase-matched points ($\Delta\beta \approx 0$) for idler and signal photons (shown in left and right insets respectively)

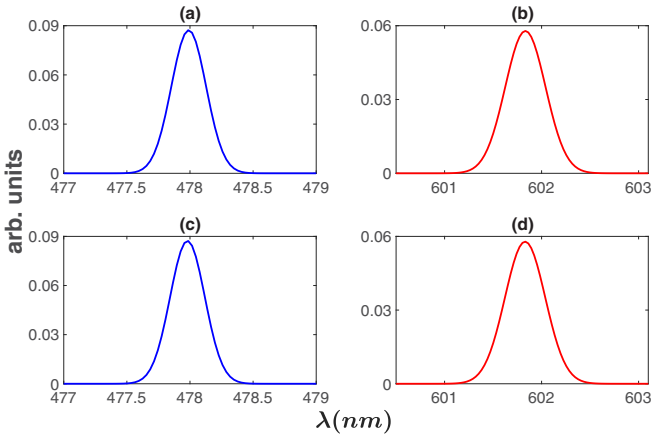

FIG. 3. The spectral shape of the first modes corresponding to first process: (a) $|h_{a_1}(\lambda_i)|^2$, (b) $|g_{a_1}(\lambda_s)|^2$, and second process (c) $|h_{b_1}(\lambda_i)|^2$, (d) $|g_{b_1}(\lambda_s)|^2$.

For the sake of simplicity, only constituent-frequency degenerate processes a and b (see Fig. 4) of first configuration are treated comprehensively. Figure 2 illustrates the phase-matching curves and phase-matching points for idler and signal photons. In Table II, eigenvalues of decomposed JSA's $f_{\mathrm{a}}(\omega_s, \omega_i)$ and $f_{\mathrm{b}}(\omega_s, \omega_i)$ are shown.

Intensity of only first two modes in spectral domain for both processes are depicted in Fig. 3 due to highest probability of occurrence, ≈97.4%. For a typical Gaussian JSA, Schmidt modes overlap in both spectral and temporal domain; i.e., they are their own Fourier transforms.

Before moving on to the spatial characterization, it is noteworthy to point out that the spectral (temporal) shape of the photons are Gaussian, and hence they are optimal for linear optical quantum information processing [32].

V. SPATIAL QUBIT CHARACTERIZATION

In this section, we introduce the density matrix formalism, which is the most convenient theoretical tool for quantum information protocols. In moving forward and describing observable quantities for subsystems of a composite system via reduced density matrices, we parametrize the two-photon wave function in the spatial (position) representation with two-dimensional transverse positions (x_s, y_s) and (x_i, y_i) of the respective photons, signal and idler, given by

$$\psi(x_{s,i}, y_{s,i}; \omega_{s,i}) = f(\omega_s, \omega_i)[\eta_1 \mathrm{LP}_{11}(x_s, y_s)\mathrm{LP}_{01}(x_i, y_i) + \eta_2 \mathrm{LP}_{01}(x_s, y_s)\mathrm{LP}_{11}(x_i, y_i)], \quad (22)$$

where $f(\omega_s, \omega_i) = f_a(\omega_s, \omega_i) = f_b(\omega_s, \omega_i)$, since they overlap in the spectral domain, see Fig. 4. A straightforward calculation shows that single-photon reduced density matrix for the spatial coordinate y in the case of signal photon by tracing out the appropriate variables is given by

$$\hat{\rho}_s = \int dx_s' dy_s' d\bar{y}_s [|\eta_1|^2 \mathrm{LP}_{11}(x_s', y_s')\mathrm{LP}_{11}^*(x_s', \bar{y}_s) + |\eta_2|^2 \mathrm{LP}_{01}(x_s', y_s')\mathrm{LP}_{01}^*(x_s', \bar{y}_s)]|y_s'\rangle\langle\bar{y}_s|, \quad (23)$$

where orthonormality of the transverse modes and normalization of the JSA are utilized. The representation of signal photon reduced density matrix $\rho_s(y, \check{y}) = \langle y|\hat{\rho}_s|\check{y}\rangle$ is

$$\rho_s(y, \check{y}) = \int dx_s' [|\eta_1|^2 \mathrm{LP}_{11}(x_s', y)\mathrm{LP}_{11}^*(x_s', \check{y}) + |\eta_2|^2 \mathrm{LP}_{01}(x_s', y)\mathrm{LP}_{01}^*(x_s', \check{y})]. \quad (24)$$

Note that the reason we restrict ourselves to only one spatial coordinate y is because the basis transverse modes (LP_{01} and LP_{11}) exhibit opposite parity in that coordinate. The reduced density matrix $\rho_i(y, \check{y})$ for an idler photon can also be calculated congruently. The Hilbert space operator $\hat{\rho}$ can

TABLE II. First three eigenvalues $\varrho_{\mathrm{a}_n}^2$ and $\varrho_{\mathrm{b}_n}^2$ of process a and process b, respectively.

	$\varrho_{\mathrm{a}_n}^2$	$\varrho_{\mathrm{b}_n}^2$
$n = 1$	0.9740	0.9742
$n = 2$	0.0253	0.0252
$n = 3$	0.0007	0.0006

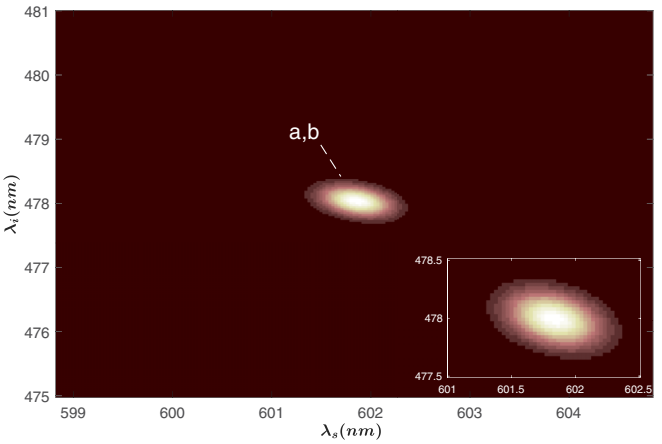

FIG. 4. Joint spectral intensity (JSI) of two processes are overlapped significantly, the bottom right inset is an enlargement of JSIs of the processes to illustrate phase-matched points.

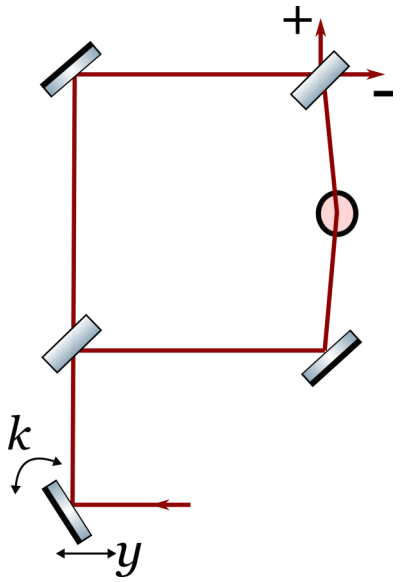

FIG. 5. Mach-Zehnder interferometer includes an image rotator (rounded object) to invert spatially one of the interfering beams and a steering mirror to determine the phase-space point (y, k) for measuring the Wigner function.

be transformed to the experimentally accessible phase-space Wigner function defined for the signal photon alone as [33]

$$\mathrm{W}_s(\mathbf{r},\mathbf{k}) = \frac{1}{\pi^2}\mathrm{Tr}[\langle\Psi|\hat{\mathbb{1}}_i \otimes \hat{\Pi}_{\mathbf{r},\mathbf{k}}|\Psi\rangle], \tag{25}$$

where $\hat{\mathbb{1}}$ is the identity operator and displaced parity operator $\hat{\Pi}_{\mathbf{r},\mathbf{k}}$ is defined as

$$\begin{aligned}\hat{\Pi}_{\mathbf{r},\mathbf{k}} &= \int d\mathbf{r}_0 \exp(-2i\mathbf{k}.\mathbf{r}_0)|\mathbf{r}-\mathbf{r}_0\rangle\langle\mathbf{r}+\mathbf{r}_0| \\ &= \int d\mathbf{k}_0 \exp(-2i\mathbf{r}.\mathbf{k}_0)|\mathbf{k}+\mathbf{k}_0\rangle\langle\mathbf{k}-\mathbf{k}_0|, \end{aligned} \tag{26}$$

where $\mathbf{r} = [x, y]$ is the two-dimensional spatial vector and $\mathbf{k} = [k_x, k_y]$ is the transverse wave vector representing the phase-space position and momentum values.

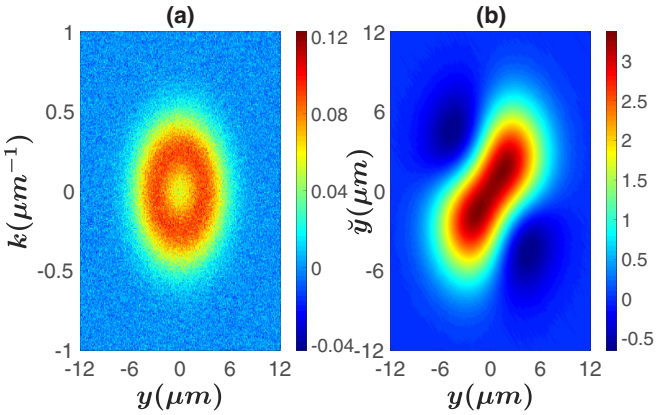

FIG. 6. (a) Noisy single-photon Wigner function with a signal-to-noise ratio (SNR) of 10, $|\eta_1|^2 = 0.45$, and $|\eta_2|^2 = 0.55$. (b) Single-photon density matrix obtained from the noisy Wigner function.

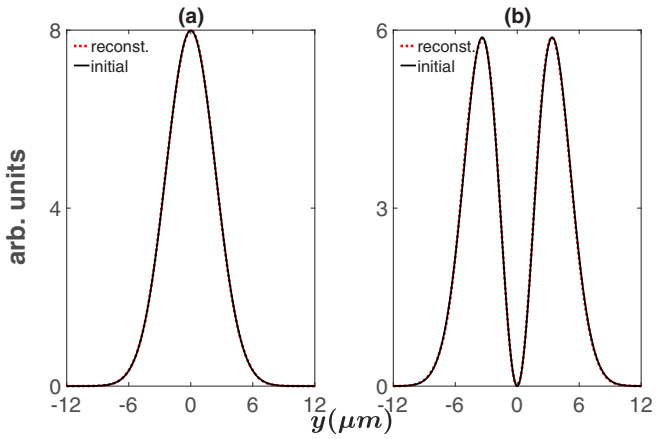

FIG. 7. Spatial profiles of (a) $|u_s^{01}|^2$ and (b) $|u_s^{11}|^2$ basis modes reconstructed from the Wigner function compared with their initial forms.

The displaced parity operator performs a reflection about the phase-space point $(\mathbf{r}, \mathbf{k})$. For a single spatial coordinate, $\mathrm{W}_s(y, k)$ can equivalently be expressed in the form related to reduced density matrix [34]

$$W_s(y,k) = \frac{1}{\pi}\int d\xi \exp(-2ik\xi)\rho_s(y+\xi, y-\xi). \tag{27}$$

Next, we investigate inverting the interferometer-based realization of the spatial Wigner function. The position argument of the Wigner function is defined by displacing the input beam with respect to the interferometer axis, whereas wave-number k dependency is proportional to the tilt of the input beam [35]; see Fig. 5. Accordingly, the reduced density matrix can be calculated with the help of inverse formula of Eq. (27).

$$\rho_s(y,\check{y}) = \int dk \exp(ik(y-\check{y}))W_s((y+\check{y})/2, k). \tag{28}$$

In order to gain further insight into the reduced density matrix and identify spatial qubit basis modes, we add Gaussian noise with standard deviation equal to 0.1 of the maximum absolute value of the Wigner function suggested in Ref. [8], and obtain the reduced density matrix with the help of Eq. (28), as shown in Fig. 6. In what follows, the reconstructed density matrix can be decomposed into eigenvalues to obtain basis modes

$$\rho_s(y,\check{y}) = \sum_p \varsigma_p u_p(y) u_p^*(\check{y}). \tag{29}$$

In Fig. 7, we compare the initial and reconstructed basis states corresponding to the two highest eigenvalues. They show remarkably good agreement despite the presence of noise and considering only the y spatial coordinate greatly simplifies practical implementations.

VI. CHSH INEQUALITY

Entanglement is one of the most prominent findings of quantum mechanics that disagrees with classical intuition and

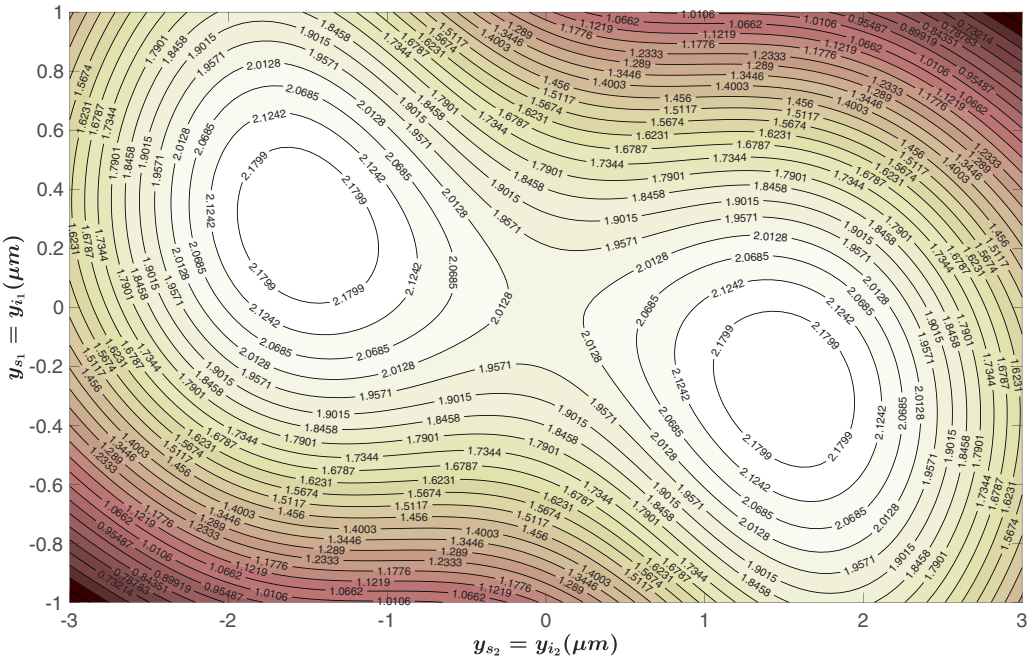

FIG. 8. Contour plot of the CHSH inequality for different alignments $y_{s_1} = y_{i_1}$ and $y_{s_2} = y_{i_2}$. Values greater than 2 indicate violation of CHSH inequality.

predicts the violation of CHSH inequality. In essence, CHSH inequality rules out the possibility of persisting memory of the interaction in a sense, between two separate quantum bodies forming a single quantum system, regardless of the distance. What gives rise to entanglement is the conservation of physical properties in the generation process. These physical properties or their conjugate variables that lead to nonclassical correlation are themselves indications of entanglement. In this scenario, conservation of the involved photons momentum gives birth to nonclassical momentum and position correlation.

The original CHSH inequality relies on dichotomic outcomes of the measurements performed on seperate subsystems. Displaced parity operator $\hat{\Pi}_{\mathbf{r},\mathbf{k}}$ that has two eigenvalues ± 1 can be used to test violation of CHSH inequality. It is sufficient to carry out this procedure in one dimension. Hence, the quantum correlation function can be written as

$$E(y_s, k_s; y_i, k_i) = \langle \Psi | \hat{\Pi}_{y_s,k_s} \otimes \hat{\Pi}_{y_i,k_i} | \Psi \rangle. \tag{30}$$

A straightforward calculation yields

$$\begin{aligned} E(y_0, k_0; y_1, k_1) = \int d\mathbf{r}_s d\mathbf{r}_i d\omega_s d\omega_i \psi(y_0 + y_s, x_s, y_1 + y_i, x_i; \\ \times \omega_s, \omega_i) \psi^*(y_0 - y_s, x_s, y_1 - y_i, x_i; \omega_s, \omega_i) \\ \times \exp(-2i(k_0 y_s + k_1 y_i)), \end{aligned} \tag{31}$$

where $\mathbf{r}_s = (x_s, y_s)$ and $\mathbf{r}_i = (x_i, y_i)$ are the transverse integration plane parameters. The CHSH inequality can be constructed for the joint transverse-spatial state for photons parametrized with (y_s, k_s) and (y_i, k_i) as follows:

$$\begin{aligned} |E(y_{s_1}, k_{s_1}; y_{i_1}, k_{i_1}) + E(y_{s_1}, k_{s_1}; y_{i_2}, k_{i_2}) \\ + E(y_{s_2}, k_{s_2}; y_{i_1}, k_{i_1}) - E(y_{s_2}, k_{s_2}; y_{i_2}, k_{i_2})| \leqslant 2. \end{aligned} \tag{32}$$

The problem is to find proper settings (y_{s_1}, k_{s_1}), (y_{s_2}, k_{s_2}), (y_{i_1}, k_{i_1}), and (y_{i_2}, k_{i_2}) that allow the given state to violate this inequality. Only displacing input beam with respect to the interferometer axis without tilting it provides a scheme for violation: $k_{s_1} = k_{s_2} = k_{i_1} = k_{i_1} = 0$. In the rest of the paper, k dependency of the correlation function will be omitted for brevity of notation, $E(y_s; y_i)$. The maximum value of constructed combination of correlation function is optimized over displacement variables $y_{s_1} = y_{i_1}$ and $y_{s_2} = y_{i_2}$ in Fig. 8.

In the experimental realization of the scheme, idler and signal photons are subjected to simultaneous separated interferometric measurements, where the displacement is applied. The two outputs of the interferometer corresponding to two possible results depending on the parity of the photon are collected and directed to a detector. Correlation function $E(y_s; y_i)$ is estimated between the parties of the two photons as a function of their respective displacements via

$$E(y_s; y_i) = \frac{C(+_s, +_i) - C(-_s, +_i) - C(+_s, -_i) + C(-_s, -_i)}{C(+_s, +_i) + C(-_s, +_i) + C(+_s, -_i) + C(-_s, -_i)}, \tag{33}$$

where C is the coincidence count rate recorded between different pairs of detectors.

VII. CONCLUSIONS

In this paper, we have theoretically analyzed spontaneously arisen spatially entangled photon pairs in a GIMF. We have presented different phase-matching configurations to achieve different degree of spatial entanglement and examined their JSA's to illuminate the meaning of spectral purities and corresponding Schmidt modes.

Spatial qubits in only one dimension in which basis transverse fiber modes have opposite parities have been

characterized via introducing density matrix formalism. We have investigated experimentally accessible single-photon Wigner function for determining the basis modes via a simple inverting interferometer with a steering mirror to scan phase-space points. The relation between spatial quantum correlation function and two-particle Wigner function has been demonstrated explicitly to verify entanglement through violation of CHSH inequality.

All these studies show that GIMFs are strong candidates for responding to every need in the field of quantum information technologies as a photon pair generation platform. Also, the results of the paper will open opportunities for controlling rich correlated spatiotemporal dynamics of photons and pave the way for further optical-fiber-based quantum information investigations and applications.

[1] P. G. Kwiat, E. Waks, A. G. White, I. Appelbaum, and P. H. Eberhard, Phys. Rev. A **60**, R773(R) (1999).

[2] X. Li, P. L. Voss, J. E. Sharping, and P. Kumar, Phys. Rev. Lett. **94**, 053601 (2005).

[3] W. P. Grice, A. B. U'Ren, and I. A. Walmsley, Phys. Rev. A **64**, 063815 (2001).

[4] P. J. Mosley, J. S. Lundeen, B. J. Smith, P. Wasylczyk, A. B. U'Ren, C. Silberhorn, and I. A. Walmsley, Phys. Rev. Lett. **100**, 133601 (2008).

[5] O. Cohen, J. S. Lundeen, B. J. Smith, G. Puentes, P. J. Mosley, and I. A. Walmsley, Phys. Rev. Lett. **102**, 123603 (2009).

[6] C. K. Law and J. H. Eberly, Phys. Rev. Lett. **92**, 127903 (2004).

[7] F. Just, A. Cavanna, M. V. Chekhova, and G. Leuchs, New J. Phys. **15**, 083015 (2013).

[8] M. Jachura, M. Karpiński, K. Banaszek, D. Bharadwaj, J. Lugani, and K. Thyagarajan, Phys. Rev. A **95**, 032322 (2017).

[9] H. Pourbeyram and A. Mafi, Phys. Rev. A **94**, 023815 (2016).

[10] K. Garay-Palmett, D. Cruz-Delgado, F. Dominguez-Serna, E. Ortiz-Ricardo, J. Monroy-Ruz, H. Cruz-Ramirez, R. Ramirez-Alarcon, and A. B. U'Ren, Phys. Rev. A **93**, 033810 (2016).

[11] D. Gloge and E. A. J. Marcatalli, Bell Syst. Tech. J. **52**, 1563 (1973).

[12] B. Franz and H. Bülow, Phot. Tech. Lett. **24**, 1363 (2012).

[13] J. F. Clauser, M. A. Horne, A. Shimony, and R. A. Holt, Phys. Rev. Lett. **23**, 880 (1969).

[14] A. Mafi, J. Lightwave Tech. **30**, 2803 (2012).

[15] R. H. Stolen, M. A. Bösch, and C. Lin, Opt. Lett. **6**, 213 (1981).

[16] B. J. Smith, P. Mahou, O. Cohen, J. S. Lundeen, and I. A. Walmsley, Opt. Express **17**, 23589 (2009).

[17] K. Inoue, J. Lightwave Tech. **10**, 1553 (1992).

[18] X. Li, J. Chen, P. Voss, J. Sharping, and P. Kumar, Opt. Express **12**, 3737 (2004).

[19] R. H. Stolen, J. E. Bjorkholm, and A. Ashkin, Appl. Phys. Lett. **24**, 308 (1974).

[20] M. F. Saleh, B. E. A. Saleh, and M. C. Teich, Phys. Rev. A **79**, 053842 (2009).

[21] C. Leary, L. Baumgardner, and M. Raymer, Opt. Express **17**, 2435 (2009).

[22] E. Mukamel, K. Banaszek, I. A. Walmsley, and C. Dorrer, Opt. Lett. **28**, 1317 (2003).

[23] F. Poletti and P. Horak, J. Opt. Soc. Am. B **25**, 1645 (2008).

[24] B. Fang, O. Cohen, J. B. Moreno, and V. O. Lorenz, Opt. Express **21**, 2707 (2013).

[25] Y. Zhang, R. Spiniolas, K. Shinbrough, B. Fang, O. Cohen, and V. O. Lorenz, Opt. Express **27**, 19050 (2019).

[26] C. K. Law, I. A. Walmsley, and J. H. Eberly, Phys. Rev. Lett. **84**, 5304 (2000).

[27] R. Loudon, *The Quantum Theory of Light* (Oxford University Press, Oxford, UK, 1973).

[28] B. Bell, A. McMillan, W. McCutcheon, and J. Rarity, Phys. Rev. A **92**, 053849 (2015).

[29] E. Nazemosadat, H. Pourbeyram, and A. Mafi, J. Opt. Soc. Am. B **33**, 144 (2016).

[30] J. W. Fleming, Appl. Opt. **23**, 4486 (1984).

[31] A. G. White, D. F. V. James, P. H. Eberhard, and P. G. Kwiat, Phys. Rev. Lett. **83**, 3103 (1999).

[32] P. P. Rohde, T. C. Ralph, and M. A. Nielsen, Phys. Rev. A **72**, 052332 (2005).

[33] N. Gonzalez, G. Molina-Terriza, and J. P. Torres, Phys. Rev. A **80**, 043804 (2009).

[34] W. P. Schleich, *Quantum Optics in Phase Space* (Wiley, Weinheim, 2001).

[35] B. J. Smith, B. Killett, M. G. Raymer, I. A. Walmsley, and K. Banaszek, Opt. Lett. **30**, 3365 (2005).